Transgenic zebrafish modeling low-molecular-weight proteinuria and lysosomal storage diseases

Check for updates

see commentary on page 1097

Zhiyong Chen[1], Alessandro Luciani[1], José María Mateos[2], Gery Barmettler[2], Rachel H. Giles[3,4], Stephan C.F. Neuhauss[5] and Olivier Devuyst[1]

OPEN

[1]Institute of Physiology, University of Zurich, Zurich, Switzerland; [2]Center for Microscopy and Image Analysis, University of Zurich, Zurich, Switzerland; [3]Department of Nephrology and Hypertension, Hubrecht Institute, Utrecht, The Netherlands; [4]University Medical Center Utrecht, Utrecht, The Netherlands; and [5]Institute of Molecular Life Sciences, University of Zurich, Zurich, Switzerland

Epithelial cells lining the proximal tubule of the kidney reabsorb and metabolize most of the filtered low-molecular-weight proteins through receptor-mediated endocytosis and lysosomal processing. Congenital and acquired dysfunctions of the proximal tubule are consistently reflected by the inappropriate loss of solutes including low-molecular-weight proteins in the urine. The zebrafish pronephros shares individual functional segments with the human nephron, including lrp2a/megalin-dependent endocytic transport processes of the proximal tubule. Although the zebrafish has been used as a model organism for toxicological studies and drug discovery, there is no available assay that allows large-scale assessment of proximal tubule function in larval or adult stages. Here we establish a transgenic *Tg(lfabp::¹/₂vdbp-mCherry)* zebrafish line expressing in the liver the N-terminal region of vitamin D-binding protein coupled to the acid-insensitive, red monomeric fluorescent protein mCherry (¹/₂vdbp-mCherry). This low-molecular-weight protein construct is secreted into the bloodstream, filtered through the glomerulus, reabsorbed by receptor-mediated endocytosis and processed in the lysosomes of proximal tubule cells of the fish. Thus, our proof-of-concept studies using zebrafish larvae knockout for *lrp2a* and *clcn7* or exposed to known nephrotoxins (gentamicin and cisplatin) demonstrate that this transgenic line is useful to monitor low-molecular-weight proteinuria and lysosomal processing. This represents a powerful new model organism for drug screening and studies of nephrotoxicity.

Translational Statement

A series of congenital or acquired disorders can cause proximal tubule dysfunction, reflected by the inappropriate loss of solutes, including low-molecular-weight proteins in the urine. The zebrafish pronephros shares individual functional segments with the human nephron, and it has been used as a model organism for toxicologic studies and drug discovery. We established a transgenic zebrafish line expressing a 50-kilodalton red fluorescent reporter protein (¹/₂vdbp-mCherry), which allows large-scale assessment of proximal tubule function in larval or adult stages. Proof-of-concept studies demonstrate that this transgenic line is useful for monitoring the low-molecular-weight proteinuria and lysosomal processing and is thus a powerful new model organism for drug screening and nephrotoxicity studies.

Correspondence: *Olivier Devuyst, Institute of Physiology, University of Zurich, Winterthurerstrasse 190, CH-8057, Zurich, Switzerland. E-mail: olivier.devuyst@uzh.ch*

The proximal tubule (PT) of the kidney plays a key role in homeostasis, via the reabsorption and processing of a large amount of filtered solutes through specialized transport systems. In physiological conditions, the epithelial cells lining the PT reabsorb the filtered low-molecular-weight (LMW) proteins (MW up to that of albumin, ∼69 kilodalton [kDa]), including hormones, vitamins and their binding proteins, enzymes, immunoglobulin light chains, as well as drugs and toxins via apical receptor-mediated endocytosis and lysosomal processing. This pathway is particularly developed in PT cells, ensuring that human urine is virtually devoid of ultrafiltered plasma proteins under physiological conditions.[1] Congenital or acquired disorders targeting the endolysosomal system in PT cells cause an inappropriate loss of LMW proteins and solutes in the urine, which can culminate in renal Fanconi syndrome leading to severe clinical manifestations, including renal failure, growth retardation, rickets, and kidney stones.[2,3] Detecting specific LMW proteinuria is the most consistent and sensitive indicator of PT dysfunction of genetic and toxic origin.[4,5]

The overall conservation of nephron segment patterning has established the zebrafish as a prominent model organism for kidney diseases and drug discovery.[6,7] In particular, the proximal convoluted tubule segment of the zebrafish pronephros is remarkably similar to the human nephron.[8] The

proximal convoluted tubule cells show the typical characteristics of reabsorbing epithelia (brush border, infoldings of basolateral plasma membrane, abundant mitochondrial network, formation of tight junctions), express the endocytic receptors megalin and cubilin, and possess lrp2a/megalin-dependent endocytic transport activity.[9] Zebrafish models of drug toxicity,[10] or genetic disorders targeting the endosomal–lysosomal pathway, including Donnai-Barrow syndrome,[11] Lowe syndrome,[12,13] and cystinosis,[14,15] support the use of zebrafish pronephros to investigate the endolysosomal system in PT cells.

In general, evaluation of toxicity of chemical compounds in zebrafish relies on visual examination of larval features (e.g., body size, shape) and morphology of internal organs,[16,17] whereas assessment of PT function relies on visualization of the uptake of injected LMW fluorescent tracers.[9,12] However, these assays are either indirect or limited by technical concerns (e.g., injection, visualization), can be difficult to quantify, and can be affected by quenching of fluorescence within acidic endolysosomal vesicles. As they are labor-intensive, the injection methods do not allow large-scale assessment of PT dysfunction in larvae or adult zebrafish models. Detecting biomarkers in fish urine is difficult, as such markers are diluted in the pool,[18] and filtration/processing of endogenous LMW proteins has not been characterized. We hypothesized that these difficulties could be overcome with a transgenic zebrafish reporter line expressing a fluorescent, LMW protein amenable to PT endocytosis and processing. The vitamin D binding protein (VDBP) is secreted from liver hepatocytes into the bloodstream, filtered through the glomerulus, and entirely reabsorbed by PT cells via megalin-mediated endocytosis.[19] Increased urinary levels of VDBP are used to detect a variety of acute and chronic disorders affecting the kidney PT.[20–24]

Based on the availability of specific tools for gene editing and kidney PT investigation, we have generated and characterized transgenic zebrafish vdbp reporter lines for analysis of LMW proteinuria in congenital and acquired PT disorders. By combining genetic models and exposure to known toxins, we provide proof-of-concept evidence that substantiates the value of such zebrafish lines for large-scale screens of kidney PT function.

RESULTS

Assessment of the endolysosomal pathways in zebrafish models

In order to explore the endolysosomal pathways in zebrafish PT, we generated mutant knockout lines for *lrp2a* (coding for megalin) and *clcn7* (coding for the lysosomal channel ClC-7) using transcription activator–like effector nucleases (TALEN) technology. Two mutant lines were identified—*lrp2a*[del8/del8] and *clcn7*[del4/del4]—with small deletions in target exons resulting in premature stop codons and truncated proteins (Supplementary Figures S1 and S2). The homozygous mutant lines displayed normal Mendelian ratios at birth, no developmental defects during the larval stage, normal fertility, and

no visible anomalies, except for the observation of an enlarged eye globe in *lrp2a* homozygous adult mutant fish (Supplementary Figure S1).

In vivo endocytic assays were performed after i.v. injection of 18.4-kDa β-lactoglobulin-Cy5 (to measure receptor-mediated endocytosis) and 10-kDa dextran-Alexa Fluor 647 (to measure fluid-phase endocytosis) in 56-hour post-fertilization (hpf) zebrafish larvae with green fluorescent pronephric tubules [transgenic *Tg(cdh17::GFP)*; Figure 1a–c]. Injected β-lactoglobulin-Cy5 was taken up within 20 minutes by pronephric PT cells of *lrp2a*^{+/+} larvae, whereas virtually no fluorescent signal was observed in *lrp2a*[del8/del8] larvae (*lrp2a*^{+/+}: 11.3 ± 0.4 vs. *lrp2a*[del8/del8]: 0.3 ± 0.1, $P < 0.001$; Figure 1a). A similar defect in the uptake of 10-kDa dextran by pronephric PT cells was observed at 60 minutes in *lrp2a*[del8/del8] larvae (*lrp2a*^{+/+}: 3.9 ± 0.4 vs. *lrp2a*[del8/del8]: 0.5 ± 0.1, $P < 0.001$; Figure 1b). Ultrastructure analysis of PT cells by transmission electron microscopy showed a significant reduction in the number of endocytic vesicles in *lrp2a*-deficient larvae, compared to *lrp2a*^{+/+} PT cells (*lrp2a*^{+/+}: 40.5 ± 4.6 vs. *lrp2a*[del8/del8]: 19.6 ± 3.4, $P < 0.001$; Figure 1c). Morphologic analysis using the endosome reporter line *Tg(PiT1::GFP-rab5aa)* revealed green fluorescent protein (GFP) fluorescence enriched at the apical side of PT cells in *lrp2a*^{+/+} larvae, which was absent in *lrp2a*[del8/del8] larvae (*lrp2a*^{+/+}: 18.6 ± 3.7 vs. *lrp2a*[del8/del8]: 9.6 ± 1.0, $P < 0.05$; Figure 1d).

The lysosomal processing was analyzed by *in vivo* pulse-chase experiments in 4 days postfertilization (dpf) *clcn7*^{+/+} and *clcn7*[del4/del4] transgenic *Tg(cdh17::GFP)* larvae after i.v. injection of β-lactoglobulin-Cy5. The β-lactoglobulin-Cy5 signal was located at the subapical pole of pronephric PT cells in both *clcn7*^{+/+} and *clcn7*[del4/del4] lines at 20 minutes (Figure 1e, left panels) and up to 1 hour (middle panels) post-injection. At 4 hours post-injection, the pronephric PT cells of *clcn7*[del4/del4] larvae accumulated considerable quantities of fluorescent ligand, whereas it was completely degraded in *clcn7*^{+/+} larvae (*clcn7*^{+/+}: 39 ± 7 vs. *clcn7*[del4/del4]: 876 ± 100, $P < 0.01$; Figure 1e, right panels). In parallel, enlarged electron-dense vesicles were observed by transmission electron microscopy in PT cells of *clcn7*-deficient larvae, as compared to controls (Figure 1f). These results show that specific defects in endocytosis (*lrp2*) and lysosomal processing of the internalized ligand (*clcn7*), with corresponding ultrastructural changes, can be detected in pronephric PT cells of larvae with genetic defects along the endolysosomal pathway.

Generation and characterization of transgenic *Tg(lfabp::¹/₂vdbp-mCherry)* line

Injection of fluorescent low-molecular-weight (LMW) tracer-like β-lactoglobulin-Cy5 is labor-intensive and not easy to accomplish for high-throughput functional assay. Both human VDBP and zebrafish vdbp contain 2 homologous ALBUMIN domains I and II (Supplementary Figure S3), which participate in vitamin D sterol-binding.[25] To create a novel, genetically encoded endocytic LMW reporter protein (Figure 2a), we
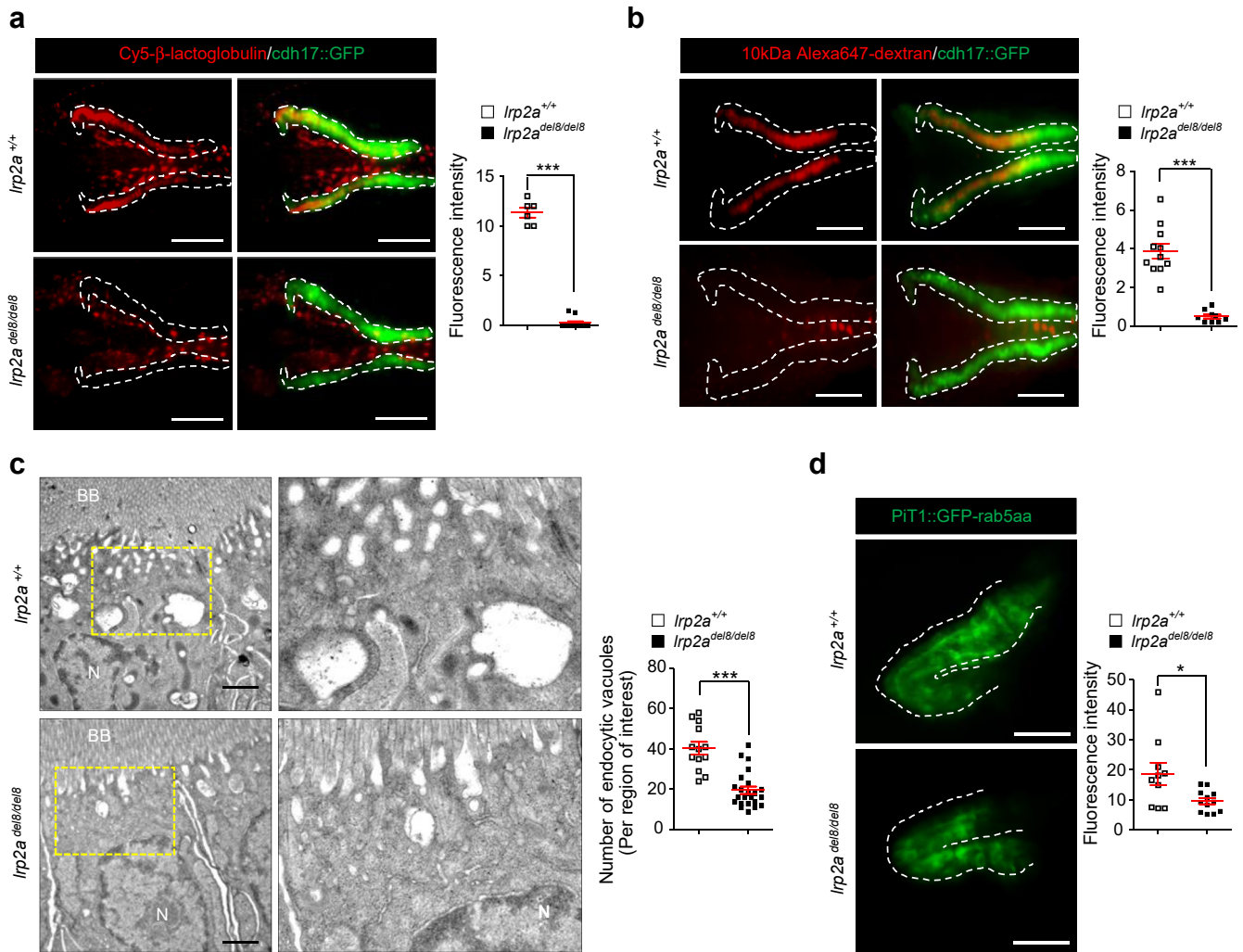
Figure 1 | Assessment of endolysosomal pathways in zebrafish models. (**a**) *Irp2a*$^{+/+}$ and *Irp2a*$^{del8/del8}$ zebrafish embryos expressing *cdh17::GFP* (green, pronephric tubule marker) were injected at 56-hour postfertilization (hpf) with β-lactoglobulin-Cy5. At 20 minutes after the tracer injection, zebrafish larvae were imaged by a light sheet fluorescence microscope. Shown are representative micrographs demonstrating the defective endocytosis of β-lactoglobulin-Cy5 in pronephric tubules of *Irp2a* zebrafish and quantifications of the Cy5 fluorescent signal; $n = 6$ (*Irp2a*$^{+/+}$) and $n = 11$ (*Irp2a*$^{del8/del8}$). Bar = 40 μm. (**b**) *Irp2a*$^{+/+}$ and *Irp2a*$^{del8/del8}$ zebrafish embryos expressing *cdh17::GFP* (green, pronephric tubule marker) were injected at 56 hpf with 10-kDa Alexa Fluor 647-Dextran. At 60 minutes after the tracer injection, the zebrafish embryos were imaged. Representative micrographs demonstrate the defective endocytosis of Alexa Fluor 647-Dextran in pronephric tubules of *Irp2a* zebrafish larvae and quantifications of the fluorescent signal; $n = 11$ (*Irp2a*$^{+/+}$) and $n = 9$ (*Irp2a*$^{del8/del8}$). Bar = 40 μm. (**c**) Representative electron micrographs showing loss of endocytic vesicles in proximal tubules (PTs) of *Irp2a* zebrafish larvae at 4 days postfertilization (dpf) and quantifications of the number of endocytic vacuoles. Yellow squares contain images at a higher magnification. $n = 6$ (*Irp2a*$^{+/+}$) and $n = 7$ (*Irp2a*$^{del8/del8}$). Bar = 1 μm. (**d**) Whole-mount imaging of PT in *Irp2a* zebrafish larvae expressing *PiT1::GFP-rab5aa* (green, endosome marker) at 4 dpf. Shown are representative micrographs demonstrating loss of GFP fluorescence enrichment at the the apical side of PT cells in *Irp2a* zebrafish and quantifications of GFP fluorescence intensity; $n = 10$ (*Irp2a*$^{+/+}$) and $n = 12$ (*Irp2a*$^{del8/del8}$). Bar = 40 μm. (Continued)

cloned the N-terminal 207aa-region containing the full ALBUMIN domain I of zebrafish vdbp protein (referred to as "$^1/_2$vdbp") and fused the latter with the open reading frame of the acid-insensitive fluorophore mCherry (Figure 2b; Supplementary Figure S4). As the promoter of the *fabp10a* gene (coding for liver-type fatty acid binding protein 10a or lfabp) is sufficient to modulate liver expression in zebrafish,[26] the 3.1-kb 5′ flanking sequence of the *lfabp* promoter was cloned to drive the expression of $^1/_2$vdbp-mCherry in liver (Figure 2b).

We next analyzed the synthesis and processing of the endogenous $^1/_2$vdbp-mCherry in stable transgenic

Tg(lfabp::$^1/_2$vdbp-mCherry) larvae. The expression of $^1/_2$vdbp-mCherry in transgenic zebrafish was confirmed by reverse-transcription polymerase chain reaction (Figure 2c), western blot (Figure 2d), and enzyme-linked immunosorbent assay (ELISA; Figure 2e) in larval lysate and/or in isolated liver and kidney tissue. Live microscopy validated signal for $^1/_2$vdbp-mCherry in the liver (Figure 2f and g), blood vessels—especially the caudal vein (Figure 2f), and PT connected to the glomerulus visualized in *wt1b::GFP* transgenic fish (Figure 2h). Within pronephric PT cells, the uptaken $^1/_2$vdbp-mCherry co-localized with the lysosome marker ctns-EGFP,
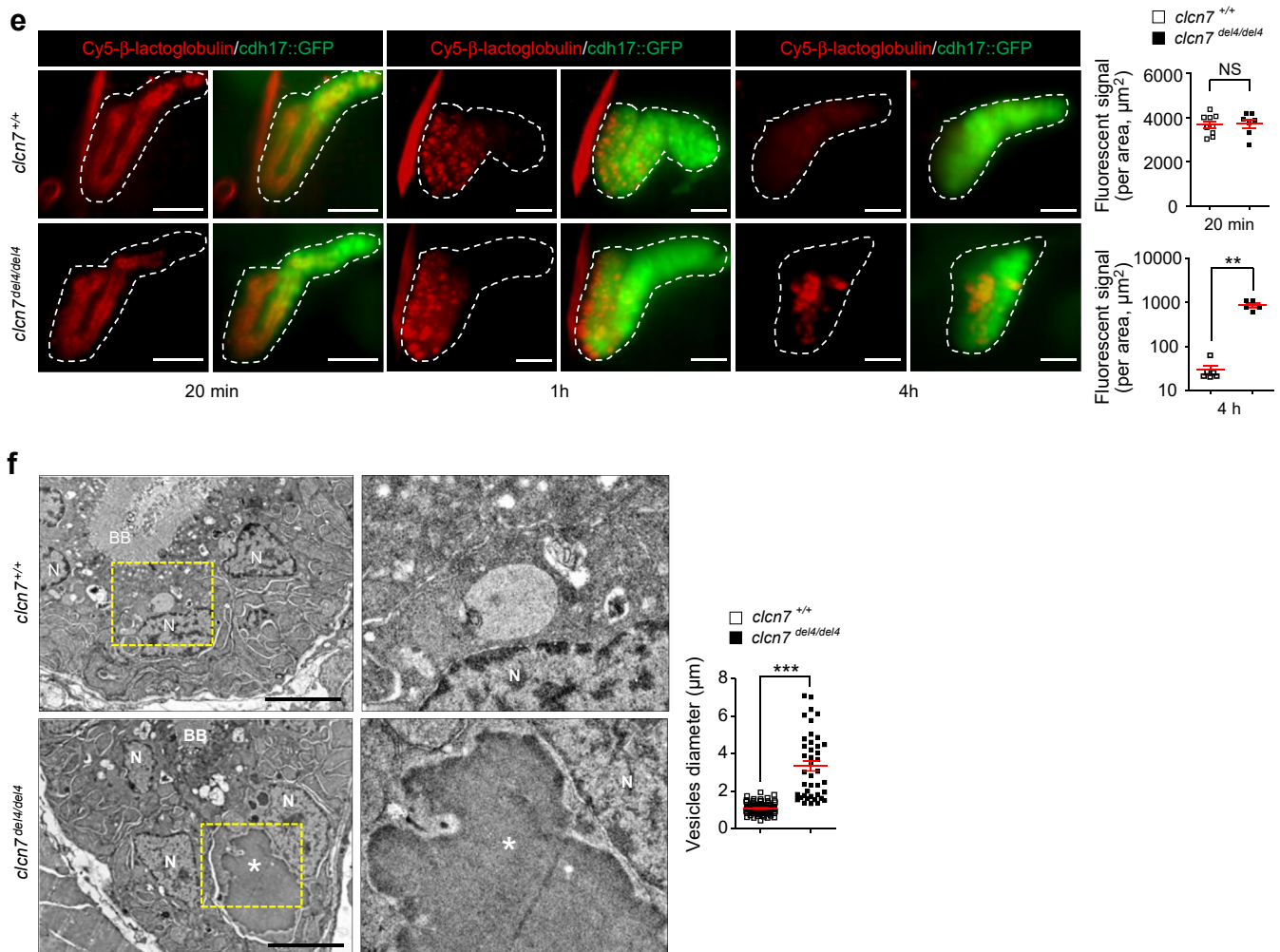
Figure 1 | (Continued) (**e**) *clcn7*^{+/+} and *clcn7*[del4/del4] larvae expressing *cdh17::GFP* (green, pronephric tubule marker) were injected at 4 dpf with β-lactoglobulin-Cy5. At the indicated times after the tracer injection, the zebrafish larvae were imaged. Representative micrographs demonstrate the accumulation of the endocytosed ligand in the PT of *clcn7* zebrafish and quantifications of the Cy5 fluorescent signal; $n = 10$ (*clcn7*^{+/+}) and $n = 7$ (*clcn7*[del4/del4]) for the early time point; and $n = 6$ (*clcn7*^{+/+}) and $n = 5$ (*clcn7*[del4/del4]) for the late time point. Bar = 40 μm. (**f**) Representative electron micrographs showing the accumulation of large electron-dense vesicles in PTs of *clcn7* zebrafish at 4 dpf and quantifications of the diameter of electron-dense vesicles; $n = 6$ (*clcn7*^{+/+}) and $n = 5$ (*clcn7*[del4/del4]). Yellow boxes contain images at a higher magnification. White asterisks indicate enlarged electron-dense vesicles. Bar = 5 μm. Plotted data represent mean ± SEM. Nonparametric Mann-Whitney test, *$P < 0.05$, **$P < 0.01$, ***$P < 0.001$ relative to *lrp2a*^{+/+} or *clcn7*^{+/+} zebrafish. BB, brush border; N, nucleus; NS, nonsignificant. To optimize viewing of this image, please see the online version of this article at www.kidney-international.org.

as confirmed by confocal microscopy analysis of cryosections (Figure 2i). These data demonstrate that ¹/₂vdbp-mCherry produced in the liver of *Tg(lfabp::¹/₂vdbp-mCherry)* larvae is filtered, reabsorbed, and processed in PT cells similar to endogenous LMW proteins.

Analysis of the clearance of recombinant 6His-tagged ¹/₂vdbp-mCherry revealed that almost 70% of tracer was removed from blood 30 minutes after injection, whereas the reabsorbed fluorescent ligand was completely degraded in PT cells 120 minutes post-injection (Supplementary Figure S5).

Of note, the reabsorption pattern of the endogenous ¹/₂vdbp-mCherry (Figure 2g) differs from the exogenous tracer β-lactoglobulin-Cy5 (Figure 1e). This observation was confirmed by injecting β-lactoglobulin-Cy5 in double transgenic *Tg(lfabp::¹/₂vdbp-mCherry/cdh17::GFP)* larvae: the

endogenous ¹/₂vdbp-mCherry was mainly uptaken by the early PT segment, and the injected β-lactoglobulin-Cy5 was reabsorbed by the late portion of PT (Supplementary Figure S6).

PT dysfunction causes low-molecular-weight proteinuria in transgenic reporter zebrafish

We next used genetic and toxic models to validate the excretion of ¹/₂vdbp-mCherry in urine as an indicator of PT dysfunction in the transgenic *Tg(lfabp::¹/₂vdbp-mCherry)* larvae system (Figure 3a). Imaging of (megalin) *lrp2a*-deficient *Tg(lfabp::¹/₂vdbp-mCherry)* larvae revealed a major decrease in the ¹/₂vdbp-mCherry signal in the *lrp2a*[del8/del8] pronephros compared to *lrp2a*^{+/+} larvae (*lrp2a*^{+/+}: 12.1 ± 2.1 vs. *lrp2a*[del8/del8]: 3.4 ± 0.6, $P < 0.001$; Figure 3b), confirming the PT endocytic defect. The defective PT uptake was
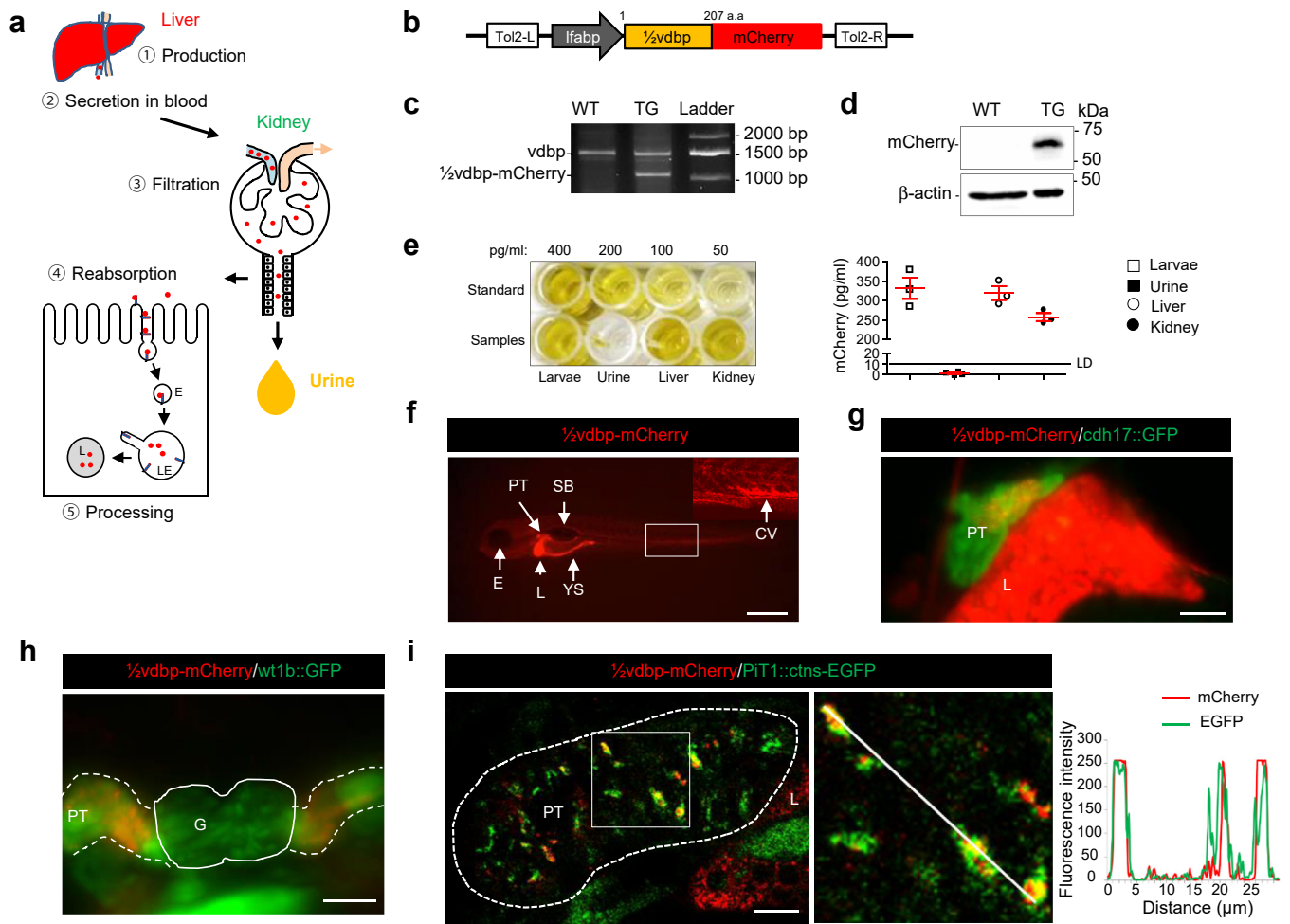
Figure 2 | Generation and characterization of transgenic *Tg(lfabp::¹/₂vdbp-mCherry)* zebrafish reporter line. (**a**) Model depicting the fate of ¹/₂vdbp-mCherry under normal conditions: ¹/₂vdbp-mCherry (~50 kDa) is (*1*) produced in liver, (*2*) secreted into the bloodstream, (*3*) filtered by the glomerulus, (*4*) reabsorbed via receptor-mediated endocytosis by proximal tubule (PT) cells, and (*5*) processed within endolysosomes. E, endosome; LE, late endosome; L, lysosome. (**b**) Vector construction of *lfabp::¹/₂vdbp-mCherry*: the N-terminal 207 amino acids of zebrafish vdbp peptide is fused to mCherry and expressed under the control of the liver-specific *lfabp* promoter. Tol2-L and Tol2-R motifs represent the Tol2 transposon left and right arms, which enable excision of the plasmid and integrate the construct into the genome. *lfabp*, promoter of liver-type fatty acid binding protein; ¹/₂vdbp, N-terminal 207 amido acids of zebrafish vdbp peptide. (**c**) Transcript levels of endogenous *vdbp* and transgene ¹/₂*vdbp-mCherry* were analyzed by reverse transcription polymerase chain reaction in liver isolated from wild-type (WT) and transgenic (TG) adult zebrafish. Upper band: endogenous vdbp; lower band: ¹/₂vdbp-mCherry. (**d**) Western blotting of mCherry protein in liver from WT and TG adult zebrafish. (**e**) Enzyme-linked immunosorbent assay and quantification of ¹/₂vdbp-mCherry in whole lysates derived from zebrafish larvae (lane 1), in urine derived from zebrafish larvae (lane 2), and in lysates obtained from liver and kidney (lanes 3 and 4, respectively). LD, limit of detection. (**f**) Live imaging of transgenic larvae showing mCherry fluorescence (red) in the liver (L), blood vessel, and PT of transgenic zebrafish larvae at 4 days postfertilization (dpf). The red signal in yolk sac (YS) is from autofluorescence. White square indicates image at higher magnification. Arrows indicate the eye (E); PT; L; swim bladder (SB); YS; and caudal vein (CV). Bar = 500 μm. (**g**) Zebrafish larvae co-expressing *lfabp::¹/₂vdbp-mCherry* (red) and *cdh17::GFP* (green, pronephric tubule marker) were imaged at 5 dpf by a light sheet fluorescence microscope. Representative micrographs showing the localization of mCherry signal in L and PT of zebrafish larva. Bar = 50 μm. (**h**) Zebrafish larvae co-expressing *lfabp::¹/₂vdbp-mCherry* (red) and *wt1b::GFP* (green, glomerulus [G] and PT marker) were imaged at 5 dpf. ¹/₂vdbp-mCherry is uptaken by PTs connecting to the glomerulus. Bar = 40 μm. (**i**) Cryosections of fixed transgenic larvae co-expressing *lfabp::¹/₂vdbp-mCherry* and *PiT1::ctns-EGFP* (green, lysosomal marker) were imaged by confocal microscopy. Shown are representative micrographs demonstrating the co-localization of ¹/₂vdbp-mCherry and ctns-EGFP in PT cells and quantifications of mCherry and EGFP fluorescence intensities. The white line indicates the area where fluorescence intensities are quantified for both mCherry and EGFP by using ImageJ (National Institutes of Health, Bethesda, MD). Yellow indicates co-localization. Bar = 10 μm. To optimize viewing of this image, please see the online version of this article at www.kidney-international.org.

paralleled by a 20-fold increase in urinary levels of ¹/₂vdbp-mCherry measured by ELISA (*lrp2a*$^{+/+}$: 2.5 ± 0.3 pg/ml vs. *lrp2a*$^{del8/del8}$: 62.1 ± 11.8 pg/ml, *P* < 0.001; Figure 3c).

Zebrafish larvae have been used previously to study the nephrotoxicity of cisplatin and gentamycin, which induce

acute kidney injury in a dosage-dependent manner.[10] We first treated *Tg(lfabp::¹/₂vdbp-mCherry)* larvae with 1.5 mM cisplatin. As expected, exposure to cisplatin induced a defective development of swim bladder in 26.0% of treated larvae, compared to 6.9% for untreated controls (Figure 3d).
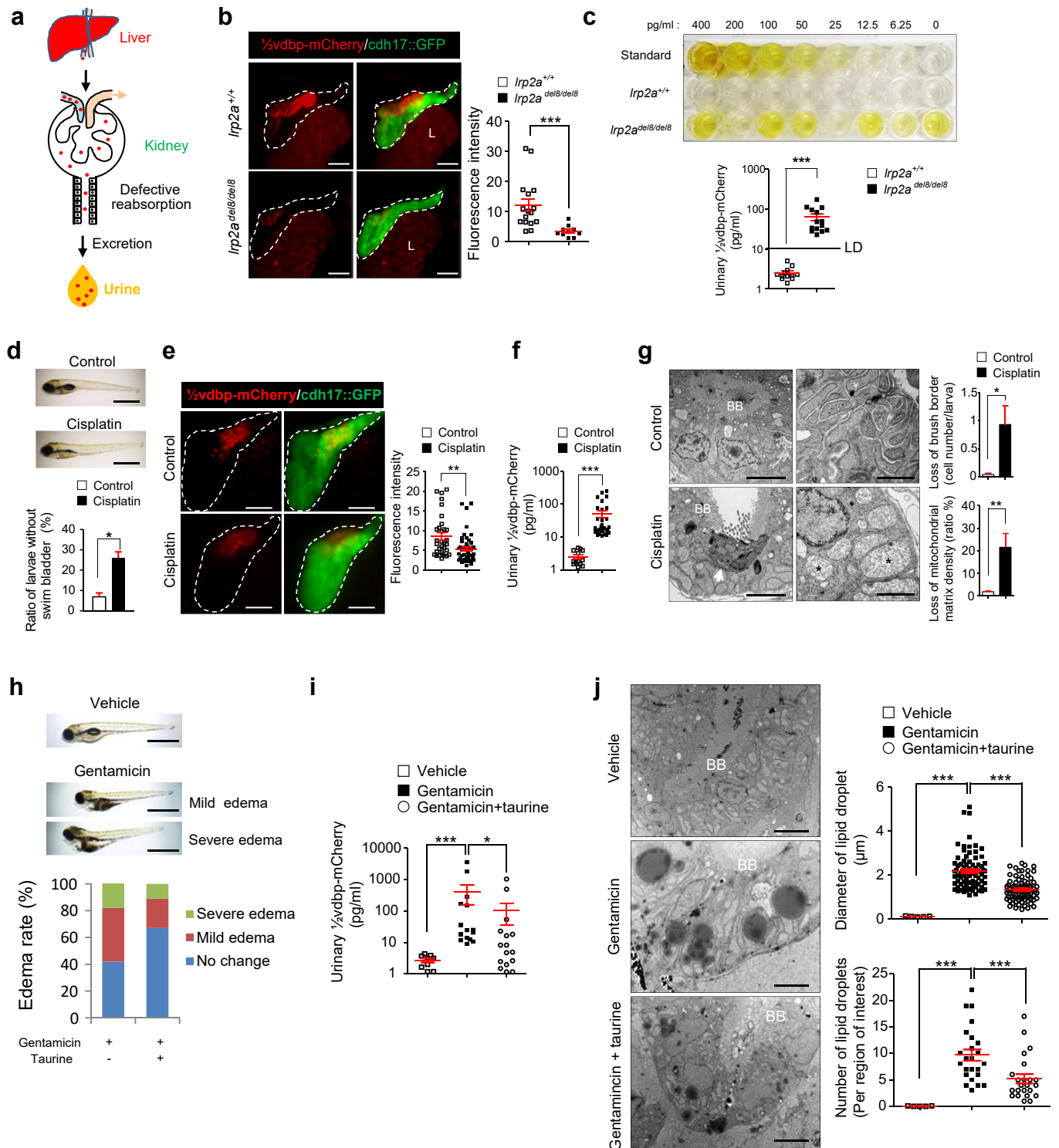
Figure 3 | Failure of receptor-mediated endocytosis leads to urinary excretion of ½vdbp-mCherry. (**a**) Model depicting the fate of ½vdbp-mCherry in endocytosis-deficient conditions: ½vdbp-mCherry is not reabsorbed by proximal tubule (PT) cells and is ultimately excreted in the urine. (**b**) $lrp2a^{+/+}$ and $lrp2a^{del8/del8}$ zebrafish larvae co-expressing *lfabp::½vdbp-mCherry* and *cdh17::GFP* (green, pronephric tubule marker) were imaged *in vivo* at 4 days postfertilization (dpf) by a light sheet fluorescence microscope. Shown are representative micrographs demonstrating the defective endocytosis of ½vdbp-mCherry in *lrp2a* zebrafish and quantifications of ½vdbp-mCherry fluorescent signal in PT; $n =$ 16 ($lrp2a^{+/+}$) and $n = 10$ ($lrp2a^{del8/del8}$). Bar = 40 μm. L, liver. (**c**) Enzyme-linked immunosorbent assay (ELISA) and quantification of the urinary ½vdbp-mCherry showing loss of the endocytic ligand in urine collected from *lrp2a* zebrafish larvae; $n = 12$ ($lrp2a^{+/+}$) and $n = 14$ ($lrp2a^{del8/del8}$). LD, limit of detection. (**d**) Morphology of zebrafish embryos treated at 2 dpf with 1.5 mM cisplatin for 4 hours and semiquantitative scoring of developmental defects of swim bladder at 4 dpf. $n = 3$ independent experiments. Bar = 1 mm. (**e**) Zebrafish embryos co-expressing *lfabp::½vdbp-mCherry* and *cdh17::GFP* (green, pronephric tubule marker) exposed to cisplatin were imaged *in vivo* at 5 dpf. Representative micrographs demonstrate the defective endocytosis of ½vdbp-mCherry in cisplatin-treated transgenic larvae and quantifications of mCherry (continued)

Three days after exposure, cisplatin-treated larvae showed a significantly decreased mCherry fluorescent signal in PT cells (untreated control: 8.6 ± 0.9 vs. cisplatin-treated group: 5.4 ± 0.5, $P < 0.01$; Figure 3e), paralleled by a 20-fold increase in urinary levels of $^1/_2$vdbp-mCherry (untreated control: 2.6 ± 0.3 pg/ml vs. cisplatin-treated group: 50.7 ± 11.9 pg/ml, $P < 0.001$; Figure 3f). As cisplatin is known to induce mitochondrial dysfunction,[27] we analyzed global mitochondrial respiration, which showed a significant decrease of oxygen consumption rate in cisplatin-treated versus control larvae (data not shown). Ultrastructural studies revealed a partial loss of the brush border, loss of mitochondrial matrix, and mitochondrial swelling in PT cells of cisplatin-treated larvae (Figure 3g), as described previously.[28,29]

Aminoglycoside antibiotics such as gentamicin are internalized in PT cells via megalin, causing PT dysfunction and structural damage.[30,31] Gentamicin-induced acute tubular damage can be prevented by taurine administration in rat models.[32] We exposed *Tg(lfabp::$^1/_2$vdbp-mCherry)* larvae to gentamicin alone or co-injected with taurine in a 1:4 molar ratio. Gentamicin-injected larvae showed mild (40%) and severe (19%) edema associated with body curvature at 2 days post-injection, compared to 22% (mild) and 11% (severe) of gentamicin-taurine co-injected larvae (Figure 3h). Analysis of urine collected at 2 days post-injection revealed high levels of $^1/_2$vdbp-mCherry in gentamicin-injected larvae compared to control larvae (gentamicin: 480 ± 258 pg/ml vs. vehicle: 2.7 ± 0.4 pg/ml, $P < 0.001$). Co-injection of taurine with gentamicin resulted in a significant attenuation of the urinary excretion of $^1/_2$vdbp-mCherry (105.7 ± 71.7 pg/ml, $P < 0.05$ vs. gentamicin alone; Figure 3i). Ultrastructural analysis showed the accumulation of lipid droplets in PT cells of gentamicin-treated larvae, which was also partially rescued by taurine co-injection (number of lipid droplets: vehicle, 0, vs. gentamicin, 9.4 ± 1.9, vs. gentamicin + taurine, 5.2 ± 1.4, $P < 0.001$; Figure 3j). Western blotting data showed that the production level of $^1/_2$vdbp-mCherry was not affected by *lrp2a* knockout or pharmacologic treatment with either cisplatin or gentamicin (Supplementary Figure S7). Taken together, these data demonstrate that genetic and toxic models of PT dysfunction are associated with a significant loss of $^1/_2$vdbp-mCherry in the urine of the *Tg(lfabp::$^1/_2$vdbp-mCherry)* larvae, which can be monitored by ELISA. The urinary levels of $^1/_2$vdbp-mCherry reflect the severity of the tubular damage and the effect of protective strategies.

Transgenic zebrafish reporter for lysosomal storage diseases
Once internalized by receptor-mediated endocytosis in PT cells, LMW proteins are delivered to early and late endosomes, and finally to lysosomes for enzymatic degradation in an acidic environment. As the mCherry remains fluorescent in an acidic environment, we hypothesized that $^1/_2$vdbp-mCherry could be useful for monitoring lysosomal dysfunction in PT cells (Figure 4a). Given that the *clcn7$^{del4/del4}$* larvae are a model of lysosomal storage diseases (see above; Figure 1e–g), we first analyzed the processing of $^1/_2$vdbp-mCherry in *clcn7$^{+/+}$* and *clcn7$^{del4/del4}$* transgenic *Tg(lfabp::$^1/_2$vdbp-mCherry)* larvae. As compared to *clcn7$^{+/+}$* larvae, the accumulation of mCherry in PT cells was detected in *clcn7$^{del4/del4}$* homozygous mutants, with both significantly increased mCherry fluorescence intensity (*clcn7$^{+/+}$*: 22 ± 4.0 vs. *clcn7$^{del4/del4}$*: 75.9 ± 6.1, $P < 0.001$) and enlarged mCherry-positive vesicles (*clcn7$^{+/+}$*: 10.8 ± 1.3 μm^2 vs. *clcn7$^{del4/del4}$*: 29.5 ± 2.0 μm^2, $P < 0.001$; Figure 4b). Reintroduction of zebrafish *clcn7* mRNA in homozygous mutant larvae partially rescued both the fluorescence intensity (*clcn7$^{del4/del4}$* + *clcn7* mRNA: 47.2 ± 4.0, $P < 0.01$ vs. non-injected control) and vesicle size (19.2 ± 2.5 μm^2, $P < 0.05$ vs. non-injected control), demonstrating that the renal phenotype is specifically related to *clcn7* gene deletion. The accumulation of fluorescent ligand in the late-endosome/lysosome in PT cells of *clcn7$^{del4/del4}$* larvae was confirmed by correlative light and electron microscopy, where $^1/_2$vdbp-mCherry-positive endolysosomal compartments overlap with the electron-dense vesicles in *clcn7* mutant (Figure 4c).

We next exposed *Tg(lfabp::$^1/_2$vdbp-mCherry)* larvae to the proton pump inhibitor bafilomycin A1 (BfnA1), which impairs lysosomal acidification. After incubation with BfnA1 (20 nM for 16 hours), both fluorescence intensity (vehicle: 18.0 ± 3.1 vs. BfnA1: 36.9 ± 2.9, $P < 0.01$) and total fluorescence area (vehicle: 158 ± 21 μm^2 vs. Bfn A1: 333 ± 37 μm^2, $P < 0.01$) were significantly increased in PT cells compared to vehicle-treated controls (Figure 4d). Western blotting data showed that the production level of $^1/_2$vdbp-mCherry was not affected by *clcn7* knockout or BfnA1 treatment (Supplementary Figure S7D and E). These results indicate

Figure 3 | (continued) fluorescent signal; $n = 32$ (control), $n = 47$ (cisplatin-treated group). Bar = 40 μm. (**f**) ELISA and quantifications of the urinary $^1/_2$vdbp-mCherry showing loss of the endocytic ligand in urine collected from cisplatin-treated transgenic zebrafish larvae; $n = 14$ (control), $n = 31$ (cisplatin-treated group). (**g**) Representative micrographs show loss of brush border (BB) and mitochondrial swelling in PT cells of cisplatin-treated zebrafish larvae. Arrowhead indicates epithelial cells deprived of BB. Asterisks indicate mitochondrial swelling; $n = 7$ (control), $n = 9$ (cisplatin-treated group). Bars = 5 μm in left panel and 2 μm in right panel. (**h**) Morphology of zebrafish larvae after i.v. injection of 6 μg/μl gentamicin alone, or 6 μg/μl gentamicin + 6.3 μg/μl taurine, or 0.9% NaCl vehicle solution into 2 dpf-transgenic embryos and semiquantitative scoring of phenotypical change at 4 dpf; $n = 53$ (gentamicin alone) and $n = 46$ (gentamicin + taurine). Bar = 1 mm. (**i**) ELISA and quantifications of the urinary $^1/_2$vdbp-mCherry in transgenic zebrafish larvae treated with vehicle, gentamicin alone, and gentamicin + taurine injection; $n = 9$ (vehicle), $n = 15$ (gentamicin alone), and $n = 16$ (gentamicin + taurine). (**j**) Shown are representative micrographs demonstrating lipid droplets in PTs from treated zebrafish larvae and quantifications of lipid droplets by transmission electron microscopy; $n = 5$ (vehicle), $n = 8$ (gentamicin alone), and $n = 9$ (gentamicin + taurine). Bar = 5 μm. Plotted data represent mean ± SEM. Nonparametric Mann-Whitney test, $*P < 0.05$, $**P < 0.01$, $***P < 0.001$ relative to *lrp2a$^{+/+}$* larvae or control. One-way analysis of variance followed by Kruskal-Wallis test, $*P < 0.05$, $**P < 0.01$, $***P < 0.001$ relative to gentamicin-treated larvae. To optimize viewing of this image, please see the online version of this article at www.kidney-international.org.
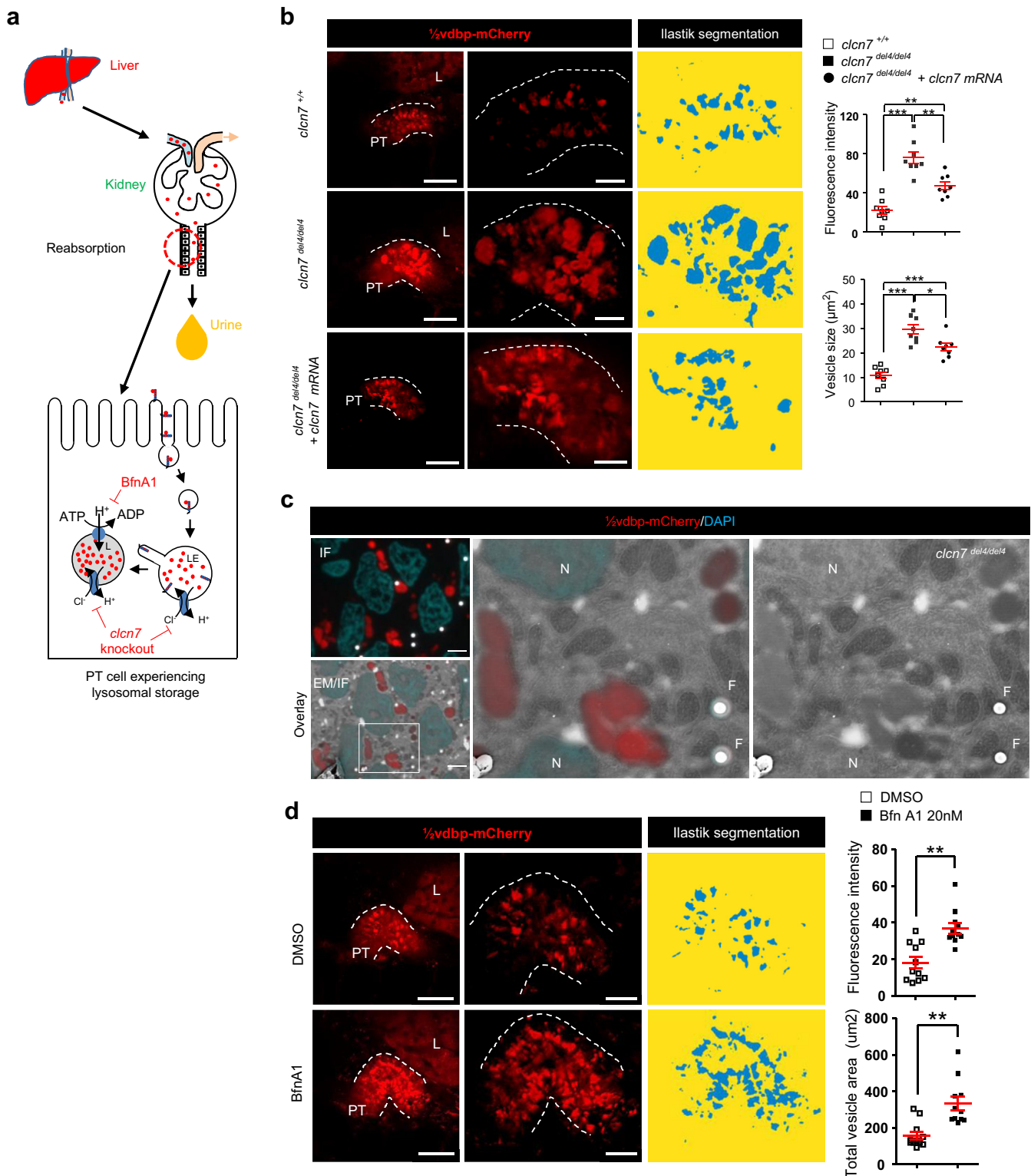
Figure 4 | Impaired lysosomal function results in defective processing of $^{1}/_{2}$vdbp-mCherry. (**a**) Model showing the fate of $^{1}/_{2}$vdbp-mCherry in response to lysosomal dysfunctions induced by either genetic (*clcn7* knockout) or pharmacologic (treatment with BfnA1) means. (**b**) Transgenic *clcn7*^{+/+} and *clcn7*[del4/del4] larvae or *clcn7*[del4/del4] injected with wild-type zebrafish *clcn7* mRNA, which express *lfabp::$^{1}/_{2}$vdbp-mCherry* in the liver, were imaged by a multiphoton fluorescence microscope at 5 days postfertilization (dpf). Shown are representative micrographs and quantifications of mCherry fluorescence intensity and vesicle size, which demonstrate the accumulation of $^{1}/_{2}$vdbp-mCherry in *clcn7* zebrafish, partially rescued by the re-introduction of wild-type *clcn7* mRNA; *n* = 8 zebrafish per group. Bar = 30 μm (left panel) and 10 μm (middle panel). (**c**) Correlative light and electron microscopy (CLEM) in proximal tubules (PTs) of *clcn7*[del4/del4] zebrafish larvae at 5 dpf expressing *lfabp::$^{1}/_{2}$vdbp-mCherry*. Ultrathin sections of fixed zebrafish larvae were imaged with a widefield fluorescence microscope and processed by super-resolution radial fluctuations analysis using ImageJ (National Institutes of Health, Bethesda, MD). The sections (continued)

that the *Tg(lfabp::¹/₂vdbp-mCherry)* larvae system can also be used to monitor the PT cell accumulation of ¹/₂vdbp-mCherry in congenital (*clcn7* knockout) or acquired (BfnA1) lysosomal dysfunction.

DISCUSSION

In order to extend the use of zebrafish as a model organism for kidney diseases, we have established a transgenic *Tg(lfabp::¹/₂vdbp-mCherry)* zebrafish line expressing the low-molecular-weight (LMW) ¹/₂vdbp-mCherry protein in the liver. Unlike the GFP-tagged full-length vdbp, the endogenously expressed ¹/₂vdbp-mCherry is secreted into the bloodstream, filtered by the glomerulus, reabsorbed by PT cells through receptor-mediated endocytosis, and processed within endolysosomes. As it is pH-insensitive, the fluorophore mCherry can be used to follow the fluorescent ligand in acidic endolysosomal compartments. Studies using genetic (knockout for *lrp2a* and *clcn7*) and pharmacologic (exposure to gentamicin and cisplatin) models demonstrate that this transgenic line is useful for monitoring LMW proteinuria and lysosomal processing in PT cells, thus representing a powerful new tool for drug screening and nephrotoxicity studies.

We first characterized the renal phenotypes of zebrafish knockout lines for the endocytic receptor megalin (*lrp2a*) and the lysosomal chloride channel ClC-7 (*clcn7*). Morphologic and functional abnormalities displayed in the pronephros of 2 knockout lines mimic the phenotypes observed in knockout mice, supporting their use to analyze the endolysosomal pathway. Imaging of *lrp2a*-deficient transgenic *Tg(lfabp::¹/₂vdbp-mCherry)* larvae revealed a major decrease in the PT endocytic uptake of the ¹/₂vdbp-mCherry tracer, resulting in the urinary excretion of ¹/₂vdbp-mCherry. These features are similar to the defects encountered in megalin-knockout mice,[33] and patients with Donnai-Barrow syndrome.[34]

Both receptor-mediated endocytosis and fluid-phase endocytosis are impaired in the *lrp2a*[del8/del8] mutant. Previous studies have demonstrated that the reabsorption of dextran, a classical marker of fluid-phase endocytosis, is impaired when receptor-mediated endocytosis is primarily abolished in zebrafish larvae.[9,11] This effect could be due to the decreased number of endocytic vesicles formed in *lrp2a*-deficient larvae, as most of the dextran is reabsorbed via such endocytic vesicles, without binding to megalin receptor but staying in the lumen fluid. Of note, the *lrp2a*[del8/del8] mutant

developed enlarged eyes, a phenotype previously described in the N-ethyl-N-nitrosurea-induced *lrp2a* mutant *bugeye* line.[35] The *lrp2a* knockout zebrafish exhibit neither developmental defects during larval stage nor a higher mortality in adults, whereas megalin-deficient newborn mice die from perinatal respiratory complications, with impaired pulmonary inflation and alveolar expansion.[36] Having gills, zebrafish do not develop lungs and are thus not exposed to respiratory abnormalities related to megalin deficiency.

The Cl⁻/H⁺ antiporter ClC-7 has been shown to be the primary chloride permeation pathway in lysosomes and important for lysosomal degradation activity,[37] whereas ClC-7 deficiency leads to lysosomal storage disease, osteropetrosis, neurodegeneration, and retinal degeneration in mouse and human.[38–40] In particular, *Clcn7*-deficient mice show severe dysmorphism and growth retardation and usually die before 7 weeks,[39] whereas survival is not affected in *clcn7* knockout zebrafish. The lack of bone phenotype in the *clcn7* knockout zebrafish could be explained by species differences in bone formation-resorption and/or the role of ClC-7 in extra-renal tissues. For instance, ClC-7 requires its β-subunit Ostm1 to support lysosomal function and bone resorption in mouse,[41] and the stability of either protein is dependent on the co-expression with its partner.[42] Although zebrafish ClC-7 protein sequence shares relatively high similarity with mouse ClC-7 (76% identical amino acids), the zebrafish ostm1 shares only 33% identical amino acids with mouse Ostm1. Such differences in protein sequence could result in different protein functions and different manifestations of the deletion of ClC-7 across species.

The presence of LMW proteins in the urine is a consistent hallmark of congenital and acquired forms of PT dysfunction.[2] The value of the LMW proteinuria assay motivated us to develop a transgenic zebrafish *Tg(lfabp::¹/₂vdbp-mCherry)* reporter line using a shortened zebrafish vdbp peptide fused to the acid-insensitive fluorophore mCherry. The transgenic *Tg(lfabp::¹/₂vdbp-mCherry)* zebrafish synthesize ¹/₂vdbp-mCherry in liver, from where it is secreted into the bloodstream, freely filtered through the glomerulus, reabsorbed by receptor-mediated endocytosis, and processed by lysosomes in PT cells. The reabsorption and lysosomal processing of ¹/₂vdbp-mCherry by PT cells can be monitored by ELISA or fluorescence imaging *in vivo*. To our knowledge, this is the first transgenic reporter line for LMW proteinuria in zebrafish. A transgenic *Tg(lfabp::vdbp-GFP)* zebrafish line in which

---

Figure 4 | (continued) are further processed for ultrastructural analyses by using low-voltage scanning electron microscopy (LVSEM). Nuclei are counterstained with 4′,6-diamidino-2-phenylindole (DAPI; blue). Bar = 2 μm. (**d**) Zebrafish larvae expressing *lfabp::¹/₂vdbp-mCherry* were exposed to BfnA1 (20 nM; for 16 hours) and imaged at 5 dpf. Shown are representative micrographs and quantifications of fluorescence intensity and total mCherry-positive area, which demonstrate the accumulation of ¹/₂vdbp-mCherry in BfnA1-treated zebrafish; *n* = 11 zebrafish per group. Bar = 30 μm (left panel) and 10 μm (middle panel). Plotted data represent mean ± SEM. One-way analysis of variance followed by Bonferroni *post hoc* test, *$P < 0.05$, **$P < 0.01$, ***$P < 0.001$ relative to *clcn7*[del4/del4] zebrafish larvae in (**b**). Nonparametric Mann-Whitney test, **$P < 0.01$ relative to vehicle-treated larvae in (**d**). ADP, adenosine diphosphate; ATP, adenosine triphosphate; BfnA1, bafilomycin A1; DMSO, dimethylsulfoxide; EM, electron microscopy; IF, immunofluorescence; F, fiducial beads used for alignment of the IF and EM images; L, lysosome; LE, late endosome; N, nucleus. To optimize viewing of this image, please see the online version of this article at www.kidney-international.org.

the 79.6-kD vdbp-GFP was synthesized in liver and secreted into the bloodstream was previously reported.[43] However, the full-length vdbp fusion protein could not leak through the zebrafish glomerular filtration barrier, so the vdbp-GFP may be useful as only a tracer for glomerular permeability, but it is not suitable for analyzing the function of PT cells. Interestingly, the endogenously produced tracer $^1/_2$vdbp-mCherry is uptaken by the early PT segment, differing from the exogenous tracer β-lactoglobulin-Cy5, which is mainly reabsorbed by the more distal portions of the proximal tubule. This observation could be due either to the chemical differences of the tracers[44] or to the saturation of reabsorption capacity of the early portion of PT by the endogenous protein in physiological conditions—so that any exogenous tracer would be uptaken by the late portion of PT.

An important aspect of our study is that the urinary excretion of $^1/_2$vdbp-mCherry (i.e., LMW proteinuria) caused by genetic (*lrp2a* deletion) or toxic (cisplatin or gentamicin) injury can be assessed reliably by its detection in the pool using an ELISA assay to quantify mCherry. The urinary $^1/_2$vdbp-mCherry is detectable in cisplatin-treated larvae that have not (yet) developed edema, showing that it is a sensitive approach to monitoring tubular dysfunction.

Treatment with gentamicin is a well-established model of acute kidney failure in rodent and zebrafish larvae.[10,32] Our data demonstrate that gentamicin treatment indeed induces LMW proteinuria as monitored by elevated urinary $^1/_2$vdbp-mCherry levels in zebrafish larvae, whereas co-administration of taurine partially rescues the LMW proteinuria and the accumulation of lipid droplets. Thus, the urinary levels of $^1/_2$vdbp-mCherry in this reporter line reflect the severity of the tubular damage and the effect of protective strategies. It has been suggested that taurine acts through several mechanisms to limit the degree of lipid peroxidation and membrane damage and increases overall mitochondrial function.[45] The mechanism underlying the rescue by taurine requires further investigation. The assessment of urinary $^1/_2$vdbp-mCherry in E3 zebrafish larval medium is a simple and non-invasive technique, useful for monitoring receptor-mediated endocytosis.

Besides monitoring LMW proteinuria, we also evaluated the potential use of the transgenic *Tg(lfabp::$^1/_2$vdbp-mCherry)* zebrafish line to analyze lysosomal storage diseases, which are characterized by the intra-lysosomal accumulation of molecules.[46] Lysosomes are catabolic centers that break down and recycle a series of substrates through the concerted action of hydrolases, acidic machinery, and membrane proteins/transporters. Accumulation of undigested material is commonly seen in kidney tubular epithelial cells in lysosomal storage diseases, such as in mice deficient in ClC-7[40] or cystinosin.[47] An important point to note is that mCherry can be followed by imaging once it reaches the acidic lysosomal compartment—as shown by its co-localization with lysosomal marker ctns-EGFP in PT epithelial cells. In transgenic *Tg(lfabp::$^1/_2$vdbp-mCherry)* zebrafish, the inhibition of lysosomal function by treatment with BfnA1 or by the deletion of

clcn7 induces the accumulation of $^1/_2$vdbp-mCherry in pronephric PT cells. These data demonstrate that the $^1/_2$vdbp-mCherry is degraded once reabsorbed by PT cells in physiological conditions, as it does the native VDBP.[19] They also substantiate the importance of lysosomal acidification and chloride homeostasis for the lysosomal processing of endocytosed ligands. A combination of the *Tg(lfabp::$^1/_2$vdbp-mCherry)* zebrafish reporter line with models of glomerular diseases will be useful for analyzing the effects of protein overloading on PT function.

In this study, we applied for the first time a correlative light and electron microscopy (CLEM) method for imaging the ultrastructure of zebrafish pronephros by scanning electron microscopy and its correlation with super-resolution light microscopy. This method has been used to analyze synapses in mouse brain tissue and mitochondrial cristae in zebrafish retina.[48] Our data show that the use of correlative light and electron microscopy, combined with super-resolution radial fluctuations analysis,[49] is a reliable and precise method for monitoring the structure and morphology of lysosomes, and by extension, autophagic vesicles in zebrafish pronephric PT cells.

In summary, the generation and proof-of-principle characterization of the transgenic *Tg(lfabp::$^1/_2$vdbp-mCherry)* zebrafish reporter line opens perspectives for the study of various aspects of congenital and acquired forms of PT dysfunction and substantiates the use of zebrafish for drug screening and nephrotoxicity studies.

METHODS

Zebrafish maintenance and chemical treatment

Zebrafish (*Danio rerio*) were kept at a day/night cycle of 14/10 hours at 28 °C. Embryos were obtained through natural spawning in the Fish Facility of the University of Zurich (Zurich, Switzerland) and raised in E3 medium containing 0.01% methylene blue. For cisplatin treatment, 2-days postfertilization (dpf) zebrafish embryos were treated with E3 medium containing 1.5 mM cisplatin (Sigma, C2210000, Buchs, Switzerland) for 4 hours and reincubated with fresh E3 medium until phenotypic analysis. The number of zebrafish larvae showing defective development of swim bladder was counted manually under a stereo microscope. For gentamicin treatment, 2-dpf zebrafish embryos were injected with 1 nl of 6 µg/µl gentamicin /0.9% NaCl solution (Sigma, G1264) alone or co-injected with 6.3 µg/µl taurine (Sigma, T0625) into the common cardinal vein after anesthesia with 0.2 mg/ml Ethyl 3-aminobenzoate methanesulfonate salt (Sigma, E10521). Embryos were immediately reincubated in fresh medium until phenotypical analysis. The morphology of zebrafish larvae was analyzed at 4 dpf under a stereo microscope and classified as follows: stage I: no morphologic change; stage II: mild edema; and stage III: severe edema.[50] Overnight urine excreted in E3 medium was collected individually after 2 days (gentamicin) or 3 days (cisplatin) of treatment. Embryos were treated with 0.003% N-Phenylthiourea (Sigma, 222909) prior to *in vivo* larval imaging. Stock solution of BfnA1 (Sigma, B1793) was prepared in dimethylsulfoxide, and zebrafish larvae were treated with E3 medium containing 20 nM BfnA1 for 16 hours at 28 °C. The experiments performed on animals were approved by the local legal authority (Veterinary Office, Canton of Zurich, Switzerland).

Generation of *lrp2a* and *clcn7* knockout zebrafish by TALEN technology

lrp2a- and *clcn7*-specific TALENS were constructed according to Golden Gate TALEN assembly protocol and using the Golden Gate TALEN and TAL Effector Kit 2.0 (Addgene Kit #1000000024, Watertown, MA). CIscript-Goldy TALEN was a gift from Daniel Carlson & Stephen Ekker (Addgene plasmid #38142), and TALENs were designed with the TAL Effector Nucleotide Targeter 2.0 software available on the Cornell University website. The *lrp2a*-TALENs target exon 75 of the zebrafish *lrp2a* gene: *lrp2a*-TALEN-Left: CCCTTTAATGTTGTTTGT and *lrp2a*-TALEN-Right: TACTGT TAGCAGTGGTGATT. The *clcn7*-TALENs target exon 7 of the zebrafish *clcn7* gene: *clcn7*-TALEN-Left: GATTATTTATTTTTTCACA and *clcn7*-TALEN-Right: AAGTGGAATCCCTCAAATAAA. The spacer of 2 TALEN target sites for both genes is 15 nucleotides, containing the *Aci*I (for *lrp2a*) and *Pst*I (for *clcn7*) restriction site used for mutant screening. The TALEN expression plasmids were linearized with BamHI and then used for *in vitro* transcription (mMESSAGE mMACHINE T3 kit, Ambion, Austin, TX). Approximately 1 nL of TALEN mRNAs (400 ng/μl) was injected into one-cell stage zebrafish embryos. After 24 hours, genomic DNA was extracted from injected embryos with normal appearance. Targeted genomic loci were amplified using primers designed to anneal approximately 430 base pairs (bp) for *lrp2a* and 240 bps for *clcn7*, and a mutant allele was detected by enzymatic digestion of the polymerase chain reaction product. The TALENs-injected adulthood (F0) zebrafish were outcrossed with wild-type zebrafish, and embryos were then raised to adulthood (F1) for screening of heterozygous carriers. Homozygous mutants (F2) were generated from incrossing of heterozygous fish for phenotypic analysis. The structure of wild-type and mutated lrp2a/megalin and chloride channel 7 proteins is predicted with the open-source tool Protter (ETH Zurich, Zurich, Switzerland).

For mRNA rescue, zebrafish *clcn7* cDNA was synthetized by reverse transcription of total RNA extracted from wild-type zebrafish kidney using iScript cDNA Synthesis Kit (BioRad, Hercules, CA) and primers *clcn7*-Fw: 5′-TATGGCCAACATCACGAAGAA-3′, *clcn7*-Rev: 5′-ATCATGTCTGTGCCAGCTGAA-3′. The *clcn7* cDNA was cloned into the pDrive TOPO cloning vector (Qiagen, Basel, Switzerland). The plasmid *pDrive-zf-clcn7* was linearized with BamHI and then used for *in vitro* transcription (mMESSAGE mMACHINE SP6 kit, Ambion), followed by Poly(A) tailing by E-PAP enzyme. Approximately 1 nL of *clcn7* mRNAs (600 ng/μl) was injected into the one-cell stage of transgenic *clcn7* knockout embryos, and the phenotype was analyzed at 5 dpf.

Generation of transgenic line with tissue-specific expression of reporter protein

The promoters of the zebrafish *fabp10a* (fatty acid binding protein 10a, liver type-fabp, or lfabp) and *slc20a1a* (PiT1, phosphate transporter 1) genes were amplified from zebrafish genomic DNA by polymerase chain reaction (Platinum Taq DNA Polymerase High Fidelity Kit, Invitrogen, Basel, Switzerland) and cloned with pENTR 5′-TOPO TA Cloning Kit (Invitrogen). EGFP-RAB7A was a gift from Gia Voeltz (Addgene plasmid #61803). Zebrafish *ctns* cDNA was synthetized by reverse transcription of total RNA extracted from zebrafish embryo using an iScript cDNA Synthesis Kit (BioRad). Zebrafish *rab5aa* cDNA was cloned from wild-type zebrafish larvae and fused with GFP coding sequence using *pCS-GFP* vector. The coding sequence of N-terminal 207 aa of the zebrafish *gc* gene (vitamin D binding protein, vdbp) was cloned from isolated zebrafish liver and fused with mCherry open reading frame using *pCS2-mCherry* vector. Middle-entry clones *pED-$\frac{1}{2}$vdbp-mCherry*, *pED-GFP-rab5aa*, *pED-EGFP-RAB7A*, and *pED-ctns* were prepared using pENTR/D-TOPO Cloning Kit (Invitrogen). The construction of plasmids *lfabp::$\frac{1}{2}$vdbp-mCherry*, *PiT1::GFP-rab5aa*, *PiT1::EGFP-RAB7A,* and *PiT1::ctns-EGFP* were realized after LR Reaction (Gateway LR Clonase II Enzyme Mix, Invitrogen; the LR Reaction is a recombination reaction between attL and attR sites, which use the LR clonase for vector construction) using destination vector *pDestTol2CG2* (Tol2 kit v1.2) with *cmlc2::EGFP* transgenesis marker, homemade 5′-entry clones and middle-entry clones, as well as 3′-entry clones *p3E-EGFPpA* and *p3E-polyA*. Plasmid DNA was co-injected with Tol2 transposase mRNA into zebrafish embryo at the one-cell stage to generate stable transgenic lines. Primers used to clone promoters and cDNA are: *lfabp*-Fw: 5′-AAATGCAAATTCTGA GCAAATGAC-3′; *lfabp*-Rev: 5′-GCTTTCTGGAGAAGCTCAACA-3′ (3527 bp); *PiT1*-Fw: 5′-CAAAGTGCCAGTAGC-CATTGA-3′; and *PiT1*-Rev: 5′-TGAATGTCTTCTGCTGGGTTG-3′ (3496 bp). *rab5aa*-Fw: 5′-AAATCAGTTCAAGCAACCTGTC-3′; *rab5aa*-Rev: 5′-GGTA ACAGAGTTTGGTGAGGG-3′ (793 bp); *ctns*-Fw: 5′-CCTTCCGCGT ATGGAGTAGC-3′; *ctns*-Rev: 5′-CCCGGTCAGGTTTTCACACT-3′ (1240 bp); *vdbp*-Fw (with *BamHI* site): 5′-TCTAACTCATCTTGA AATTATAACCAGTGGATCCTAAGAAATGATGAATGCATCTTTAAT TTTAATTTATG-3′; and *vdbp*-Rev (with *BamHI* site): 5′-CTCAGA AAAATGTTGGATCCTCTCATCTGGATTCTCTCTTGGAAAAAAC AAGA-3′.

Double transgenic zebrafish larvae were produced after incross of transgenic *Tg(lfabp::1/2vdbp-mCherry)* zebrafish with transgenic *Tg(cdh17::GFP)*, *Tg(wt1b::GFP)*, or *Tg(PiT1::ctns-EGFP)*.

Production and purification of recombinant $\frac{1}{2}$vdbp-mCherry for clearance studies

Recombinant 6xHis-tagged $\frac{1}{2}$vdbp-mCherry and (His)$_6$-fusion proteins were produced using the ExpiCHO Expression System (Thermo Fisher Scientific, Basel, Switzerland). The expression vector *pCMV-$\frac{1}{2}$vdbp-mCherry-6His* was transiently transfected into ExpiCHO-S cell in serum-free ExpiCHO Expression Medium using ExpiFectamine CHO Reagent. At 20 hours after transfection, ExpiFectamine CHO Enhancer and ExpiCHO Feed were added into the medium, which was collected for purification 3 days after transfection. The medium, supplemented with ethylenediamine tetra-acetic acid–free Protease Inhibitor Cocktail (cOmplete; Roche, Mannheim, Germany) and 1 mM phenylmethylsulfonyl fluoride was concentrated and cleaned up with Amicon Ultra-15 filter unit (PLTK Ultracel-PL Membran, 30 kDa; Merck Millipore, Cork, Ireland) and binding buffer (20 mM Tris pH 8.0, 500 mM NaCl, 5 mM imidazole, protease inhibitor , and phenylmethylsulfonyl fluoride). After ultracentrifugation (170,000 g for 1hour at 4 °C), the supernatant was purified by Ni^{2+}-affinity chromatography using HiTrap Chelating High Performance column (GE17-0408-01 SIGMA; GE Healthcare, Uppsala, Sweden) and Fast Protein Liquid Chromatography (FPLC, Bio-Rad). The recombinant $\frac{1}{2}$vdbp-mCherry-6His protein was rescued in elution buffer (20 mM tris(hydroxymethyl)-aminomethane, pH 8.0, 500 mM NaCl, 500 mM imidazole), filtered and cleaned up 3x with 30-kDa-filter unit and phosphate buffered saline (PBS) solution to remove imidazole, followed by 1x filtration with a 50-kDa-filter unit and concentration determination by using an ELISA mCherry kit.

The clearance rate of $\frac{1}{2}$vdbp-mCherry was analyzed following i.v. injection of the purified recombinant protein (single bolus injection of 1 nl of 0.3 mg/ml $\frac{1}{2}$vdbp-mCherry-6His) in transgenic larvae

expressing EGFP-RAB7A. The fluorescence signal was analyzed in the dorsal aorta at 5, 15, 30, and 60 minutes after tracer injection, and in the proximal tubule at 15 and 120 minutes post-injection.

Endocytic activity assay

Bovine β-lactoglobulin (Mr 18,400, Sigma) was labeled and purified with Cy5 TM2 Ab labelling kit (Amersham BioSciences, PA35000, Little Chalfont Buckinghamshire, UK) according to manufacturer instructions. β-lactoglobulin-Cy5 injection solution was prepared at 5 mg/mL final concentration. Transgenic *Tg(cdh17::GFP)* larvae expressing GFP in pronephric epithelial cells (Dr. Frank Bos, Utrecht, The Netherlands) were anaesthetized with 0.2 mg/mL tricaine solution in egg water, prior to injection of β-lactoglobulin-Cy5 or 10-kDa dextran-Alexa Fluor 647 (Invitrogen, D22914) into the common cardinal vein. Tracer injection into larvae blood was confirmed by immediate observation of positive fluorescent vessels. Larvae were reincubated in fresh E3 medium for 20 minutes, 1 hours, or 4 hours, followed by overnight fixation with 2% paraformaldehyde/PBS containing 0.1% tween 20.

Fluorescence microscopy

A lightsheet fluorescence microscope (ZEISS Lightsheet Z.1, Carl Zeiss Microscopy, Jena, Germany) was used to visualize the expression of transgenic reporter lines *in vivo* or in fixed larvae after tracer injection by using ×20/1.0 NA water immersion objective (W Plan APO, Zeiss). The whole-larva imaging was followed by genotype assessment before data analysis was performed. Images were processed with Imaris (Bitplane, Zurich, Switherland) to generate a maximum-intensity projection of Z-stack, which was used for the quantification of the fluorescence intensity with ImageJ (National Institutes of Health, Bethesda, MD). Quantitative analysis of fluorescent signals was performed with one whole pronephric tubule for each larva using the same setting parameters. A multiphoton fluorescence microscope (Leica TCS SP8 Upright MP FLIM; Leica Microsystems, Heerbrugg, Switzerland) was used to acquire high-resolution images to ananlyze the fluorescent vesicles in proximal tubules by using ×25/1.0 NA water immersion objective (HC IRAPO L, Leica). The excitation wavelength was 1100 nm (tunable laser) for imaging of mCherry alone, and a 925-nm tunable laser and a 1041-nm fixed-wavelength laser were used for dual-color imaging of EGFP and mCherry. The acquired data were processed by Huygens software (Scientific Volume Imaging, Hilversum, The Netherlands) for deconvolution, followed by segmentation using ilastik software (EMBL, Heidelberg, Germany) and quantification of individual vesicle size or total vesicle area for each stack using ImageJ. For co-localization analysis, fixed transgenic larvae were infiltrated with 30% sucrose at 4 °C overnight, mounted in Tissue-Tek O.C.T. Compound (TissueTek, Sakura Finetek, Alphen aan den Rijn, The Netherlands), and frozen at 80 °C. 10-μm cryosections were prepared and analyzed by a Leica SP8 upright confocal microscope with a ×40 oil immersion objective (HCX PL APO, Leica Microsystems, Wetzlar, Germany). A single Z-stack was used for quantification of GFP and mCherry fluorescence signal by ImageJ.

Transmission electron microscopy

After tail cutting, zebrafish larvae were fixed in 2.5% glutaraldehyde and 1.6% paraformaldehyde in 0.1 M cacodylate buffer, pH 7.3, overnight. After rinsing in 0.1 M cacodylate buffer, larvae were then post-fixed in 1% osmium tetroxide in cacodylate buffer for 40

minutes at room temperature and stained in 1% aqueous uranyl acetate for 1 hour at room temperature. After dehydration through a graded series of ethanol, samples were infiltrated and embedded in Epon812 (Sigma, Buchs, Switzerland) at 60 °C for 28 hours. 350-nm semi-thin sections were prepared on a Leica EM FCS ultramicrotome (Leica Microsystems) and stained by Toluidine blue solution. 60-nm ultra-thin sections were collected onto formvar-coated copper grids, stained with lead phosphate dilution in water, and analyzed on an electron microscope (Philips CM100, Philips Electron Optics, Eindhoven, The Netherlands) at 80kV. Image analysis was made using ImageJ. The vesicle number was counted manually, and the vesicle diameter is expressed as the average of membrane-to-membrane diameter based on the *x* and *y* axes.

Correlative light and electron microscopy

After removing the head and tail, zebrafish larvae were fixed in 0.05% glutaraldehyde and 4% formaldehyde in 0.1 M cacodylate buffer at 4 °C overnight. To achieve better cutting stability, the tissue pieces were embedded in 12% gelatin (local food brand, Extra Gold, Dr. Oetker) in 0.1 M phosphate buffer, pH 7.4, at 40 °C. After hardening, 1-×-1 mm pieces were cut out on ice and then incubated in 2.3 M sucrose at 4 °C. After 2 washes in 2.3 M sucrose, the tissue/gelatin pieces were stored at –20 °C or further processed in fresh 2.3 M sucrose. Tissue/gelatin pieces were mounted on a cryo pin (Leica Microsystems) and cryosectioned with a cryosectioning device (UC6, Leica Microsystems). 110-nm Tokuyasu cryosections were collected on silicon wafers (7 × 7 mm, Si-Mat Silicon Materials, Kaufering, Germany). Prior to sample collection, wafers were glow-discharged, and fluorescent beads of 170 nm (PS-SpeckTM, Thermo Fisher) were added as fiducial markers. After collection, samples were washed twice with PBS and stained with 4′, 6-diamidino-2-phenylindole for 30 seconds. The sections on wafer were then incubated in 87% glycerin (Sigma)/PBS 1:1 solution for 2 × 10 seconds and then transferred with the sections facing down to a glass-bottom petri dish (Ibidi, Gräfelfing, Germany) and imaged with a Widefield fluorescence microscope (Leica Microsystems TIRF - Leica SR GSD 3D) with a x160/1.43 NA oil immersion objective (HCX PL APO, Leica Microsystems) acquiring 1000 images per channel for the super-resolution radial fluctuations analysis. Before ultrastructural analysis, the ultrathin sections were washed with PBS, post-fixed with 0.1% glutaraldehyde in PBS for 5 minutes, and incubated with 2% methylcellulose in water at 0 °C (2 × 5 minutes). The wafers were then centrifuged at 14,100 × g for 90 seconds, heated at 40 °C for 10 minutes, mounted on a scanning electron microscopy aluminium stub with conducting carbon cement (Conductive Carbon, Plano, TX), and imaged in a scanning electron microscope (Zeiss Auriga 40 CrossBeam, Carl Zeiss Microscopy) using an acceleration voltage of 1.5 keV.[48] Fluorescence images were processed with the plugin Super-Resolution Radial Fluctuations[49] within the open-source platform Fiji. Fluorescent beads registered in the light and electron microscopy images were used for the alignment of the images with TrakEM2 (Zurich, Switzerland).[51]

Reverse-transcription polymerase chain reaction

Total RNA was extracted from liver tissue isolated from adult zebrafish using TRIzol Reagent (Invitrogen) and T10 Basic UltraTurrax Disperser (IKA, Staufen, Germany). DNAse I treatment was performed to eliminate genomic DNA contamination. One microgram of RNA was converted into cDNA using an iScript cDNA Synthesis Kit (Bio-Rad). The cDNA of *vdbp* and *1/2vdbp*-mCherry was detected by polymerase chain reaction using Phusion

High-Fidelity PCR Master Mix (New England Biolabs, Hitchin, UK) and specific primers: *vdbp*-cDNA-Fw: 5′-ATGAATGCATCTT-TAATTTTAATTTATGCTTTAATAGT-3′ (containing the start codon of vdbp cDNA) and *vdbp*-cDNA-Rev: 5′-TTCAGGCGATCTCTT-CATCCA-3′ (located on the 3′ Untranslated Transcribed Region of vdbp cDNA; for vdbp cDNA, 1459 bp), and *vdbp-mCherry*-Fw: 5′-GCATCCAGGCATTGAGCAG-3′ (located on the N-terminus of vdbp cDNA) and *vdbp-mCherry*-Rev: 5′-TTACTTGTACAGCTC GTCCATGC-3′ (containing stop codon of mCherry open reading frame; for $\frac{1}{2}$vdbp-mCherry, 1030 bp).

Western blotting

Zebrafish larval or liver tissue was homogenized in RIPA buffer (Sigma, R0278) by sonication, and protein concentration was determined using Pierce BCA Protein Assay Kit (ThermoFisher, 23225). Samples were mixed with Laemmli sample buffer and separated by sodium dodecylsulfate–odecylsulfatesulfateparated by ted under reducing conditions. After blotting onto polyvinylidene diflouride membrane and blocking with 5% nonfat milk (Bio-Rad, 1706404) diluted in PBS, the membranes were incubated overnight at 4 °C with primary antibody against mCherry (Abcam, ab167453; Cambridge, UK), β-actin (Sigma, A5441), or glyceraldehyde-3-phosphate dehydrogenase (Cell Signaling, 14C10; Leiden, The Netherlands). After being washed and incubated with peroxidase-labeled secondary antibody (Dako, Glostrup, Denmark), the membranes were visualized with ChemiDoc Touch Imaging System (Bio-Rad).

Urine collection and ELISA mCherry

Zebrafish larvae were placed in a 96-well microplate with one larvae/100 µl E3 medium/well and kept at 28 °C for 16 hours, followed by urine collection for ELISA assays. Liver and kidney tissues were extracted using 1x Cell Extraction Buffer PTR and diluted with Sample Diluent NS from the mCherry ELISA kit (Abcam, ab221829). $\frac{1}{2}$vdbp-mCherry was assayed according to manufacturer-recommended protocol, which is briefly as follows: 50 µl E3 medium containing urine was distributed to a 96-well microplate pre-coated with anti-mCherry antibody. A 50-µl mixture of capture antibody and detector antibody was added to each well and incubated at 37 °C for 1 hour. The wells were rinsed 3 times with 1× Wash Buffer PT and incubated with 100 µl of TMB Substrate at room temperature for 10 minutes. The reaction was stopped by adding 100 µl of stop solution, followed by reading the absorbance of each well at 450 nm.

Statistical analysis

The software Prism 5 (GraphPad Software, San Diego, CA) was used for all statistical analyses. The D'Agostino-Pearson normality test was applied to all data sets. For experiments with more than 2 conditions, differences between experimental groups were evaluated using one-way analysis of variance followed by Bonferroni or Kruskal-Wallis *post hoc* tests. When only 2 groups were compared, either an unpaired 2-tailed *t*-test or a Mann-Whitney test was used.

For experiments with *lrp2a* and *clcn7* lines, larvae generated from crossing heterozygous lines were used. Whole-mount imaging was done in a blinded manner, before genotype determination. Thus, the exact sample size in each experiment was variable. None of the samples was excluded from the experiment. Zebrafish embryos were randomly selected for the chemical-treatment group or control group. Statistical significance was set at $P < 0.05$.

SUPPLEMENTARY MATERIAL
Supplementary File (Word)
Figure S1.
Figure S2.
Figure S3.
Figure S4.
Figure S5.
Figure S6.
Figure S7.

REFERENCES

1. Christensen EI, Birn H, Storm T, et al. Endocytic receptors in the renal proximal tubule. *Physiology*. 2012;27:223–236.
2. van der Wijst J, Belge H, Bindels RJM, et al. Learning physiology from inherited kidney disorders. *Physiol Rev*. 2019;99:1575–1653.
3. Devuyst O, Luciani A. Chloride transporters and receptor-mediated endocytosis in the renal proximal tubule. *J Physiol*. 2015;593:4151–4164.
4. Bernard A, Lauwerys R. Low-molecular-weight proteins as markers of organ toxicity with special reference to Clara cell protein. *Toxicol Lett*. 1995;77:145–151.
5. Devuyst O, Igarashi T. Renal Fanconi syndrome, Dent disease, and Bartter syndrome. In: Thakker RV, Whyte MP, Eisman JA, Igarashi T, eds. *Genetics of Bone Biology and Skeletal Disease*. London: Academic Press, Elsevier; 2018:783–799.
6. Jerman S, Sun Z. Using zebrafish to study kidney development and disease. *Curr Top Dev Biol*. 2017;124:41–79.
7. Poureetezadi SJ, Wingert RA. Little fish, big catch: zebrafish as a model for kidney disease. *Kidney Int*. 2016;89:1204–1210.
8. Drummond IA, Davidson AJ. Zebrafish kidney development. *Methods Cell Biol*. 2016;134:391–429.
9. Anzenberger U, Bit-Avragim N, Rohr S, et al. Elucidation of megalin/LRP2-dependent endocytic transport processes in the larval zebrafish pronephros. *J Cell Sci*. 2006;119:2127–2137.
10. Hentschel DM, Park KM, Cilenti L, et al. Acute renal failure in zebrafish: a novel system to study a complex disease. *Am J Physiol Renal Physiol*. 2005;288:F923–F929.
11. Kur E, Christa A, Veth KN, et al. Loss of Lrp2 in zebrafish disrupts pronephric tubular clearance but not forebrain development. *Dev Dyn*. 2011;240:1567–1577.
12. Oltrabella F, Pietka G, Ramirez IBR, et al. The Lowe Syndrome protein OCRL1 is required for endocytosis in the zebrafish pronephric tubule. *Plos Genet*. 2015;11:e1005058.
13. De Leo MG, Staiano L, Vicinanza M, et al. Autophagosome-lysosome fusion triggers a lysosomal response mediated by TLR9 and controlled by OCRL. *Nat Cell Biol*. 2016;18:839–850.
14. Elmonem MA, Khalil R, Khodaparast L, et al. Cystinosis (ctns) zebrafish mutant shows pronephric glomerular and tubular dysfunction. *Sci Rep*. 2017;7:42583.

15. Festa BP, Chen Z, Berquez M, et al. Impaired autophagy bridges lysosomal storage disease and epithelial dysfunction in the kidney. *Nat Commun*. 2018;9:161.
16. Kari G, Rodeck U, Dicker AP. Zebrafish: an emerging model system for human disease and drug discovery. *Clin Pharmacol Ther*. 2007;82:70–80.
17. Dai YJ, Jia YF, Chen N, et al. Zebrafish as a model system to study toxicology. *Environ Toxicol Chem*. 2014;33:11–17.
18. Outtandy P, Russell C, Kleta R, et al. Zebrafish as a model for kidney function and disease. *Pediatr Nephrol*. 2019;34:751–762.
19. Nykjaer A, Dragun D, Walther D, et al. An endocytic pathway essential for renal uptake and activation of the steroid 25-(OH) vitamin D3. *Cell*. 1999;96:507–515.
20. Raggi C, Luciani A, Nevo N, et al. Dedifferentiation and aberrations of the endolysosomal compartment characterize the early stage of nephropathic cystinosis. *Hum Mol Genet*. 2014;23:2266–2278.
21. Terryn S, Tanaka K, Lengele JP, et al. Tubular proteinuria in patients with HNF1alpha mutations: HNF1alpha drives endocytosis in the proximal tubule. *Kidney Int*. 2016;89:1075–1089.
22. Mirkovic K, Doorenbos CR, Dam WA, et al. Urinary vitamin D binding protein: a potential novel marker of renal interstitial inflammation and fibrosis. *Plos One*. 2013;8:e55887.
23. Malard V, Gaillard JC, Berenguer F, et al. Urine proteomic profiling of uranium nephrotoxicity. *Biochim Biophys Acta*. 2009;1794:882–891.
24. Shoukry A, Bdeer Sel A, El-Sokkary RH. Urinary monocyte chemoattractant protein-1 and vitamin D-binding protein as biomarkers for early detection of diabetic nephropathy in type 2 diabetes mellitus. *Mol Cell Biochem*. 2015;408:25–35.
25. Swamy N, Head JF, Weitz D, et al. Biochemical and preliminary crystallographic characterization of the vitamin D sterol- and actin-binding by human vitamin D-binding protein. *Arch Biochem Biophys*. 2002;402:14–23.
26. Her GM, Yeh YH, Wu JL. 435-bp liver regulatory sequence in the liver fatty acid binding protein (L-FABP) gene is sufficient to modulate liver regional expression in transgenic zebrafish. *Dev Dyn*. 2003;227:347–356.
27. Lomeli N, Di K, Czerniawski J, et al. Cisplatin-induced mitochondrial dysfunction is associated with impaired cognitive function in rats. *Free Radic Biol Med*. 2017;102:274–286.
28. Dobyan DC, Levi J, Jacobs C, et al. Mechanism of cis-platinum nephrotoxicity: II. Morphologic observations. *J Pharmacol Exp Ther*. 1980;213:551–556.
29. Zsengeller ZK, Ellezian L, Brown D, et al. Cisplatin nephrotoxicity involves mitochondrial injury with impaired tubular mitochondrial enzyme activity. *J Histochem Cytochem*. 2012;60:521–529.
30. Raggi C, Fujiwara K, Leal T, et al. Decreased renal accumulation of aminoglycoside reflects defective receptor-mediated endocytosis in cystic fibrosis and Dent's disease. *Pflugers Arch*. 2011;462:851–860.
31. Lopez-Novoa JM, Quiros Y, Vicente L, et al. New insights into the mechanism of aminoglycoside nephrotoxicity: an integrative point of view. *Kidney Int*. 2011;79:33–45.
32. Erdem A, Gundogan NU, Usubutun A, et al. The protective effect of taurine against gentamicin-induced acute tubular necrosis in rats. *Nephrol Dial Transplant*. 2000;15:1175–1182.
33. Leheste JR, Rolinski B, Vorum H, et al. Megalin knockout mice as an animal model of low molecular weight proteinuria. *Am J Pathol*. 1999;155:1361–1370.
34. Kantarci S, Al-Gazali L, Hill RS, et al. Mutations in LRP2, which encodes the multiligand receptor megalin, cause Donnai-Barrow and facio-oculo-acoustico-renal syndromes. *Nat Genet*. 2007;39:957–959.
35. Veth KN, Willer JR, Collery RF, et al. Mutations in zebrafish lrp2 result in adult-onset ocular pathogenesis that models myopia and other risk factors for glaucoma. *Plos Genet*. 2011;7:e1001310.
36. Willnow TE, Hilpert J, Armstrong SA, et al. Defective forebrain development in mice lacking gp330/megalin. *Proc Natl Acad Sci U S A*. 1996;93:8460–8464.
37. Graves AR, Curran PK, Smith CL, et al. The Cl-/H+ antiporter ClC-7 is the primary chloride permeation pathway in lysosomes. *Nature*. 2008;453:788–792.
38. Cleiren E, Benichou O, Van Hul E, et al. Albers-Schonberg disease (autosomal dominant osteopetrosis, type II) results from mutations in the ClCN7 chloride channel gene. *Hum Mol Genet*. 2001;10:2861–2867.
39. Kornak U, Kasper D, Bosl MR, et al. Loss of the ClC-7 chloride channel leads to osteopetrosis in mice and man. *Cell*. 2001;104:205–215.
40. Kasper D, Planells-Cases R, Fuhrmann JC, et al. Loss of the chloride channel ClC-7 leads to lysosomal storage disease and neurodegeneration. *EMBO J*. 2005;24:1079–1091.
41. Lange PF, Wartosch L, Jentsch TJ, et al. ClC-7 requires Ostm1 as a beta-subunit to support bone resorption and lysosomal function. *Nature*. 2006;440:220–223.
42. Jentsch TJ. Chloride and the endosomal-lysosomal pathway: emerging roles of CLC chloride transporters. *J Physiol*. 2007;578:633–640.
43. Zhou W, Hildebrandt F. Inducible podocyte injury and proteinuria in transgenic zebrafish. *J Am Soc Nephrol*. 2012;23:1039–1047.
44. Schuh CD, Polesel M, Platonova E, et al. Combined structural and functional imaging of the kidney reveals major axial differences in proximal tubule endocytosis. *J Am Soc Nephrol*. 2018;29:2696–2712.
45. Ye HB, Shi HB, Yin SK. Mechanisms underlying taurine protection against glutamate-induced neurotoxicity. *Can J Neurol Sci*. 2013;40:628–634.
46. Parenti G, Andria G, Ballabio A. Lysosomal storage diseases: from pathophysiology to therapy. *Annu Rev Med*. 2015;66:471–486.
47. Cherqui S, Sevin C, Hamard G, et al. Intralysosomal cystine accumulation in mice lacking cystinosin, the protein defective in cystinosis. *Mol Cell Biol*. 2002;22:7622–7632.
48. Mateos JM, Barmettler G, Doehner J, et al. Direct imaging of uncoated biological samples enables correlation of super-resolution and electron microscopy data. *Sci Rep*. 2018;8:11610.
49. Gustafsson N, Culley S, Ashdown G, et al. Fast live-cell conventional fluorophore nanoscopy with ImageJ through super-resolution radial fluctuations. *Nat Commun*. 2016;7:12471.
50. Cianciolo Cosentino C, Roman BL, Drummond IA, Hukriede NA. Intravenous microinjections of zebrafish larvae to study acute kidney injury. *J Vis Exp*. 2010; pii: 2079.
51. Cardona A, Saalfeld S, Schindelin J, et al. TrakEM2 software for neural circuit reconstruction. *Plos One*. 2012;7:e38011.